The postsynaptic MAGUK scaffold protein MPP2 organises a distinct interactome that incorporates $GABA_A$ receptors at the periphery of excitatory synapses

Bettina Schmerl[1], Niclas Gimber[2], Benno Kuropka[3], Jakob Rentsch[3], Stella-Amrei Kunde[1], Helge Ewers[3], Christian Freund[3], Jan Schmoranzer[2], Nils Rademacher[1,4¤] and Sarah A. Shoichet[1¤*]

[1] Neuroscience Research Center, Charité – Universitätsmedizin Berlin, Germany

[2] Advanced Medical BioImaging Core Facility – AMBIO, Charité – Universitätsmedizin Berlin, Germany

[3] Institute of Chemistry and Biochemistry, Freie Universität Berlin, Germany

[4] German Center for Neurodegenerative Diseases (DZNE), Berlin, Germany

[¤] These authors contributed equally

* Corresponding author sarah.shoichet@charite.de

Author contributions: BS, NR, and SAS designed the study. BS, NR, BK, NG, and JR carried out experiments and imaging. BS, NG, and BK performed data analysis with the support of NR, SAK, JS, HE, CF, and SAS. BS and SAS wrote the manuscript, and BS prepared the figures. All authors reviewed the manuscript.

Abbreviations

AMPA, α-amino-3-hydroxy-5-methyl-4-isoxazolepropionic acid; DIV, days in vitro; *d*STORM, direct stochastic optical reconstruction microscopy; GABA, γ-aminobutyric acid; MAGUK, membrane-associated guanylate kinase; MPP2, membrane protein palmitoylated 2; NN, nearest neighbour; PSD postsynaptic density; SIM, structured illumination microscopy

Abstract

Recent advances in imaging technology have highlighted that scaffold proteins and receptors are arranged in sub-synaptic nanodomains. The synaptic MAGUK scaffold protein MPP2 is a component of AMPA receptor-associated protein complexes and also binds to the synaptic cell adhesion molecule SynCAM1. Using super-resolution imaging, we now show that MPP2 and SynCAM1 are situated at the periphery of the postsynaptic density. In order to explore MPP2-associated protein complexes, we used a quantitative comparative mass spectrometry approach and identified multiple $GABA_A$ receptor subunits among the novel synaptic MPP2 interactors. We further show that $GABA_A$ receptors are found together with MPP2 in a subset of dendritic spines and thus highlight MPP2 as a scaffold molecule capable of acting as an adaptor molecule that links peripheral synaptic elements critical for inhibitory regulation to central structures at the PSD of glutamatergic synapses.

Introduction

At postsynaptic sites on glutamatergic neurons, a complex arrangement of transmembrane receptors, scaffold molecules, and regulatory proteins enables the coordinated regulation of synaptic transmission (for reviews see [1-3]). Recent advances in imaging technology have highlighted that scaffold proteins and receptors are not distributed evenly throughout the postsynapse, but instead are arranged in sub-synaptic nanodomains [4]. These nanodomains are regions in which specific proteins are present at higher concentrations than in the surrounding areas, and they are individually regulated, functional units that are highly dynamic [5, 6]. The relevance of their regulation for synaptic function is becoming increasingly apparent (for reviews see [7-9]). Super-resolution imaging data from glutamatergic synapses suggest that such scaffold protein nanoclusters are responsible for concentrating glutamate receptors at particular sub-synaptic sites [5]. The incidence of these clusters seems to roughly scale with spine size, and clusters have been observed to undergo morphological plasticity [5, 10]. Sub-synaptic cluster dynamics at the postsynapse can also influence synaptic transmission, e.g. by affecting diffusion and/or trapping of neurotransmitter receptors [5, 6, 11].

We and others have recently demonstrated that MPP2 is a postsynaptic scaffold protein that is present in AMPA receptor-associated protein complexes [12-15]. Like PSD-95 and related molecules, MPP family proteins are members of the MAGUK family of scaffold molecules. Different from PSD-95 molecules, they do not bind directly to glutamate receptors or their auxiliary subunits. However, MPP2 binds directly to SynCAM1 synaptic cell adhesion molecules [13] that are positioned at the periphery of the PSD [16], suggesting that they may serve functions that differ from those of the core synaptic MAGUKs.

In this study, we have investigated this new postsynaptic MAGUK and its structural role at the PSD of glutamatergic synapses. We demonstrate that MPP2, like SynCAM1, sits at the periphery of the PSD and that it interacts with a unique set of proteins that differs significantly in composition from the set of PSD proteins binding to PSD-95 family synaptic MAGUKs. These novel interactions highlight the role of MPP2 in linking core synaptic components to transmembrane proteins and regulatory molecules with complementary functions at the periphery of the PSD. Importantly, we show that multiple $GABA_A$ receptor subunits are among the proteins that bind preferentially to the MPP2 scaffold molecule, and we show that $GABA_A$ receptors are found together with MPP2 and other classical PSD markers in a subset of dendritic spines. We thus highlight that the MPP2 scaffold molecule is capable of acting as an adaptor molecule that links important PSD protein complexes with elements critical for inhibitory regulation at the PSD of glutamatergic synapses.

Results

MPP2 and its interaction partner SynCAM1 are positioned at the periphery of the PSD

To investigate how MPP2 links the SynCAM1 cell adhesion molecules with the core PSD components, we first took advantage of diverse imaging strategies to comparatively analyse endogenous PSD-95, MPP2 and SynCAM1 proteins in primary rat hippocampal neurons (Fig 1a). Using dual-colour *d*STORM, we observe clusters of SynCAM1 in a ring-like arrangement of approximately 500 nm diameter (Fig 1b, upper panel) surrounding the PSD marked by PSD-95, which is in line with published data [17].

Next, we examined the subcellular localisation of endogenous MPP2 and found a similar bracelet-like arrangement (approximately 500 nm in diameter), of small clusters of MPP2 surrounding postsynaptic densities as marked by PSD-95 (Fig 1b, middle panel). Further, when we stained for SynCAM1 in combination with MPP2, we observe that immunofluorescence of the two proteins is indeed arranged in a similar manner: at postsynaptic sites, we observe ring-like arrangements of SynCAM1 and MPP2 clusters that associate with each other and exhibit minor overlap (Fig 1b, lower panel).

Fig 1: Clusters of SynCAM1 and MPP2 surround the postsynaptic density

(a) Widefield images of E18 primary rat hippocampal neurons fixed at DIV21 and stained for endogenous MPP2, PSD-95 and SynCAM1.

(b) E18 rat hippocampal neurons were fixed at DIV21 and subjected to immunostaining for endogenous SynCAM1, PSD-95 and/or MPP2 proteins followed by dual-colour dSTORM imaging. Protein localisations were filtered according to Thompson accuracy [18], i.e. all localisations with accuracy below 20 nm were excluded. Top: SynCAM1 (magenta) clusters surround PSD-95 (cyan). Middle: Clusters of endogenous MPP2 (magenta) show a similar bracelet-like arrangement surrounding the PSD (PSD-95, cyan). Bottom: SynCAM1 (magenta) and MPP2 (cyan).

For additional images please see supplements (S1 Fig, S2 Fig, S3 Fig).

MPP2 is located in clusters at the periphery of the postsynaptic density

To assess whether this ring-like arrangement of MPP2 and SynCAM1 clusters surrounding PSD-95 is representative for the majority of synapses (and to avoid selection bias), a quantitative 3D super-resolution approach is necessary. We therefore tested whether we could resolve ring-like MPP2 and SynCAM1 structures also using 3D multicolour structured illumination microscopy (SIM). While offering less spatial resolution compared to *d*STORM, SIM inherently produces 3-dimensional data and can easily be adapted for more than two colour channels. Indeed, 3D SIM imaging is sufficient to observe similar planar bracelet-like cluster arrangements of SynCAM1 and MPP2 surrounding central PSD-95 labelled PSDs (Fig 2a).

Fig 2: Clusters of MPP2 and SynCAM1 form bracelet-like arrangements at the edge of the postsynaptic density.

Mature (DIV21) primary rat hippocampal neurons immunostained for endogenous PSD-95 (blue, second column), MPP2 (green, third column) and SynCAM1 (red, fourth column) and subjected to 3D structured illumination microscopy (3D SIM).

(a) Most dendritic spines express all three proteins of interest (overview maximum projection, first row). A single synapse detail (second row) depicts the bracelet-like arrangements of MPP2 and SynCAM1 surrounding central PSD-95 puncta. A 3D rendering of that particular synapse in top (third row) and side view (fourth row) reveals that SynCAM1 and MPP2 clusters are arranged in an interlocked, bracelet-like form, surrounding a central cluster of PSD-95. Box sizes: overview = 7.7 µm, detail = 2.5 µm, 3D rendering = 2.8 µm.

(b) Histograms illustrating the distribution of protein cluster sizes for PSD-95 (top, blue), MPP2 (middle, green) and SynCAM1 (bottom, red). Indicated radii were calculated based on extracted cluster volumes, assuming a spherical shape. The final bin in each histogram contains summarised data for cluster sizes greater than 400 nm. Histograms reflect clusters associated with ~40,000 synapses (in 50 images from N = 3 independent experiments).

(c) 3D radial intensity profiles of PSD-95, MPP2 and SynCAM1 signals in relation to the centres of PSD-95 clusters. Plot shows averaged normalised mean ± SEM from three independent experiments (~40.000 synapses from 50 images). For details on the analysis, please see the methods.

(d) Nearest neighbour (NN) analysis of MPP2 and SynCAM1 protein clusters after 3D segmentation. NN distances from MPP2 to the nearest SynCAM1 cluster were calculated from the cluster centres (upper panel, grey bars) and cluster surfaces (lower panel). Dashed lines represent the upper and lower envelopes of complete spatial randomness (CSR). CSR was calculated by randomly distributing MPP2 within the volume and SynCAM1 on the surface of spheres of 0.8 µm diameter as indicated by the grey dotted line (mean ± SEM, 95% confidence interval, 10 simulations per synapse, N = 3 independent experiments, ~40.000 synapses from 50 images). See S4 Fig for NN analysis in the reverse direction.

Using semi-automated image segmentation (see methods) we quantitatively assessed the segmented object counts and radii as derived from the cluster volumes. In line with published data [6, 10] and our *d*STORM results, we find PSD-95 clusters over a range of expected sizes (Fig 2b, upper panel, blue). Interestingly, the majority of MPP2 (Fig 2b, middle panel, green) and SynCAM1 (Fig 2b, lower panel, red) clusters are smaller than ~100 nm in radius.

Next, we quantitatively analysed the SynCAM1 and MPP2 protein distribution in relation to PSD-95 clusters, by measuring 3-dimensional radial distribution of all three proteins around the PSD centre defined by the PSD-95 signal. The 3D radial intensity profile of PSD-95 immunofluorescence intensity drops considerably at a radial distance of ~250 nm (Fig 2c, blue curve), which is consistent with reported PSD sizes. The SynCAM1 signal (Fig 2c, red curve) is low at the centre of the postsynaptic density and highest towards the border of the PSD (radial distance of ~250 nm), which is observable here in the steep decrease in PSD-95 signal. This data is in line with the idea that clusters of SynCAM1 define the edge of the PSD and the synaptic cleft [17]. Interestingly, the 3D radial intensity profile for MPP2 is almost identical to that of SynCAM1: we observe little fluorescence towards the centre of the postsynaptic density (radial distances below 250 nm) and the highest signal at the PSD border (Fig 2c, green curve). This quantitative result validates our qualitative super-resolution observation that MPP2, like SynCAM1, is distributed at the periphery of the PSD, around the core PSD protein PSD-95.

To assess the spatial relationship of the peripheral SynCAM1 and MPP2 protein clusters, we performed nearest neighbour (NN) analysis, which interrogates the nanoscale distances of the closest SynCAM1 cluster to each MPP2 cluster, and *vice versa*. This NN analysis was performed by assessing both the distances from centre-to-centre and from surface-to-surface for each 3-dimensional object. The distance distributions were quantitatively compared to a simulated random distribution within the known volume of a postsynapse [19]. The centre-to-centre NN analysis showed that most centres of MPP2 clusters have an NN distance of 200 nm - 500 nm to centres of SynCAM1 clusters (Fig 2d, upper panel). Similar results were obtained when analysing the centre-to-centre distances of SynCAM1 clusters to the nearest MPP2 cluster (see S4 Fig), showing that the two proteins do not form one uniform cluster. The obtained range of NN distances rather corresponds to the sum of both cluster radii (average cluster sizes are below 200 nm; Fig 2b, middle and lower panel), suggesting a juxtapose association of the proteins.

To test whether the surfaces of MPP2 and SynCAM1 clusters overlap with each other, we performed a surface-to-surface NN analysis, which showed a significant accumulation of MPP2 clusters at very small distances to SynCAM1 clusters and *vice versa* (Fig 2d, lower panel). This accumulation is very prominent regarding the MPP2 clusters that are located around SynCAM1 clusters (Fig 2d, lower panel), however, it is less prominent when analysed inversely (see S4 Fig). This indicates that most MPP2 clusters are associated with SynCAM1 clusters but not *vice versa*, suggesting the existence of an additional SynCAM1 pool that is independent from the postsynaptic MPP2, which is in line with the fact that SynCAM1 is also present at presynaptic sites. In summary, these data show that MPP2 and SynCAM1 clusters are not spatially identical but tightly juxtaposed at the periphery of the PSD.

Although clusters of SynCAM1 and MPP2 are not spatially identical, their close association offers sufficient chances for molecular interaction with each other. At the same time, it highlights the possibility that other surfaces remain accessible for interactions with other proteins. This is consistent with the idea that the MAGUK scaffold protein MPP2, like PSD-95, serves as a protein-protein interaction hub and that it is able to mediate the indirect connection of multiple proteins through

143 diverse, domain-specific protein-protein interactions. In summary, our super-resolution data provide
144 evidence that MPP2 and SynCAM1 are postsynaptic proteins in a close sub-synaptic arrangement
145 sitting at the periphery of postsynaptic densities, rather than being central components of the PSD,
146 and thus highlight the potential for the scaffold protein MPP2 to mediate formation of complexes that
147 are distinct from the central nanodomains orchestrated by the neighbouring MAGUK PSD-95.

148

149 **The C-terminal SH3GK domains of MPP2 and PSD-95 interact with distinct synaptic proteins**

150 The observed peripheral synaptic localisation of MPP2 relates to that of its PDZ ligand binding partner
151 SynCAM1 [13, 16]. PSD-95 is located in central sub-synaptic nanodomains that likewise correlate with
152 the localisation of its PDZ domain-binding partners, i.e. glutamate receptors and auxiliary proteins [20-
153 23]. The SH3 and GK domains, which are typically located at the C-terminus of MAGUK scaffold proteins
154 (for overview of MPP2 and PSD-95 domain architecture see Fig 3a), also participate in scaffold complex
155 formation. Importantly, it has been shown that the GK domain of MAGUK proteins is an inactive
156 guanylate kinase [24] that has evolved into an important protein interaction domain. An
157 intramolecular interaction between the SH3 and GK domains of MAGUKs has been well-characterised,
158 and several studies also support the idea that these domains of the MAGUK protein PSD-95 are
159 involved in regulated multi-protein complex formation [25, 26]. While numerous binding partners for
160 this region of PSD-95 have been described, interactors specific for the SH3GK domain of MPP2 have
161 not been identified so far.
162 Given the observed peripheral localisation of MPP2, we hypothesised that identification of its
163 C-terminal interaction partners might illuminate protein complexes that differ from those organised
164 by the central PSD-95 scaffold molecule. To explore this idea, we performed a comparative and
165 quantitative mass spectrometry analysis (see Fig 3b for experimental design). Using bacterially
166 expressed GST-MPP2-SH3GK and GST-PSD-95-SH3GK, we pulled down SH3GK-binding proteins from
167 adult rat crude synaptosome preparations. Interacting proteins were eluted from the beads and
168 separated by SDS-PAGE. Enzymatic $^{16}O/^{18}O$-labelling was used for relative quantification of proteins by

nanoLC-MS/MS analysis. In replicate A, proteins enriched by MPP2-SH3GK carried the naturally highly abundant ^{16}O isotope, while proteins enriched by PSD-95-SH3GK were labelled by ^{18}O using $H_2{}^{18}O$ during tryptic in-gel digestion (see Fig 3b). In replicate B, labels were switched. In total, we reproducibly identified and quantified 188 proteins (see Source Data). Plotting the protein heavy/light ratios (H/L) from replicate A (Fig 3c, X-axis) against the light/heavy ratios (L/H) from replicate B (Fig 3c, Y-axis) shows proteins enriched to PSD-95-SH3GK in the first quadrant and proteins enriched to MPP2-SH3GK in the third quadrant (Fig 3c). Background proteins (not completely washed from the beads) and proteins which bind to both SH3GK constructs show ratios of about 1. From all identified proteins, 83% have been previously reported in human and/or mouse postsynaptic density preparations [27], confirming the validity of our approach for identifying true PSD proteins. Further evidence illustrating the strength of our strategy is the fact that several known interactors of PSD-95 (including e.g. Map1a, MecP2, CaMKII and Fxr1) were identified among proteins enriched in the GST-PSD-95-SH3GK pull-down (Fig 3c).

Fig 3: Identification of interactors that differentially bind to the C-terminal SH3GK modules of MPP2 and/or PSD-95.

(a) Schematic domain structures of PSD-95 and MPP2 to scale and aligned by their central PDZ domain. Both proteins contain two N-terminal domains (PDZ1+PDZ2 for PSD-95 and two L27 domains for MPP2) in addition to the C-terminal `MAGUK core´ domains PDZ-SH3-GK. Note the differences in the length of the `linker´ between PDZ and SH3 domain and of the `hook´ between SH3 and GK domains.

(b) Schematic representation of the quantitative LC-MS/MS experiment using $^{16}O/^{18}O$-labelling to identify differential interactors from adult rat brain crude synaptosomal preparations by GST pull-down of bacterially expressed GST-MPP2-SH3GK or GST-PSD-95-SH3GK.

(c) GST pull-downs were performed in duplicates with inverted labelling and 188 interacting proteins were identified and quantified by mass spectrometry passing our threshold settings. PSD-95 / MPP2 protein ratios from both replicates A and B (normalised by the ratio of GST) are plotted against each other. Proteins in the first quadrant indicate preferential enrichment to PSD-95 (ratios >> 1), while proteins in the third quadrant indicate preferential enrichment to MPP2 (ratios << 1). Proteins with ratios of ~1 show no preferential binding, and thus reflect equal binding to both baits or background proteins that were not fully removed by the washing steps. Selected novel potential interaction partners were validated by co-IP (yellow, see also S5 Fig). The most significantly enriched proteins to the GST-SH3GK construct of MPP2 (green cluster) are seven different $GABA_A$ receptor subunits.

Importantly, proteins found consistently in the MPP2 pull-downs reflect putative novel synaptic MPP2 binding proteins. Of the newly identified proteins present in the GST-MPP2-SH3GK pull-down samples (see S1 Table Source Data), most have been found in PSD preparations before [27], which is in line with our previous work highlighting MPP2 as an important postsynaptic scaffold.

Several putative novel MPP2 interaction partners were selected for validation and further study (see Fig 3c, highlighted proteins; see also Table 1 for more detail). We demonstrated that both Gnao1 and Arhgef2, proteins involved in signalling cascades relevant for postsynaptic function [28, 29], interact with MPP2 in co-immunoprecipitation assays (see S5 Fig). We also validated a clear interaction between MPP2 and the membrane-associated synaptic proteins Farp1 and Pip5k1c (S5 Fig).

Importantly, in addition to revealing previously unknown binding partners for MPP2, our comparative quantitative MS strategy provided us with important information on how the MPP2 interactome relates to that of PSD-95. Of particular interest, the set of proteins most significantly enriched in the GST-MPP2-SH3GK pull-down comprised multiple gamma-aminobutyric acid (GABA) A receptor subunits (highlighted in green in Fig 3c; see also Table 1 and Source Data). Seven different $GABA_A$ subunits, namely α1, α2, α4, β1, β2, β3, and δ, were enriched more than seven-fold. In combination, these subunits are able to form complete hetero-pentameric receptors [30, 31], illustrating the potential for MPP2 molecules to interact at multiple sites with a fully functional $GABA_A$ receptor. These results are striking, as $GABA_A$ receptors are not known to be expressed at high levels at the PSD of glutamatergic synapses.

We validated the interaction between MPP2 and the $GABA_A$ α1 subunit by co-immunoprecipitation (see Fig 4a and Table 1). In this context, it is also interesting that MPP2 also interacts with the calcium-dependent, calmodulin-stimulated protein phosphatase (Calcineurin) subunit Ppp3ca (see Fig 3c, Table 1, and S5 Fig), which is known to influence $GABA_A$ receptor signalling [32]. Together these data support the novel idea that MPP2 could be involved in $GABA_A$ receptor-mediated processes at the PSD of glutamatergic synapses.

Table 1: Validated novel interaction partners for MPP2 (for co-immunoprecipitation data see Fig 4a and S5 Fig)

Name	Uniprot Accession ID	Description	Remarks
Gnao1	GNAO_RAT	Guanine nucleotide-binding protein G(o) subunit alpha	transducer in transmembrane signalling systems
Arhgef2	ARHG2_RAT	Rho guanine nucleotide exchange factor 2	Interacts with AMPA receptors
Farp1	FARP1_RAT	FERM, ARHGEF and pleckstrin domain-containing protein 1	SynCAM interactor
Pip5k1c	PI51C_RAT	Phosphatidylinositol 4-phosphate 5-kinase type-1 gamma	Binds to FERM domains, activated by Rho / Rho GEF signaling
Ppp3ca	PP2BA_RAT	Serine/threonine-protein phosphatase 2B catalytic subunit alpha isoform	Calcineurin subunit; known $GABA_A$ R interactor
GABAA α1	GBRA1_RAT	Gamma-aminobutyric acid receptor subunit alpha-1	Predominant $GABA_A$ subunit in the brain

$GABA_A$ receptor subunits are novel synaptic interaction partners of MPP2

The proteins most significantly enriched in the MPP2-SH3GK pull-down were multiple $GABA_A$ receptor subunits. To further investigate this unexpected result, we overexpressed $GABA_A$ α1 together with full-length FLAG-MPP2. Upon pull-down of the receptor subunits with Ms-α$GABA_A$ α1 antibody, we could detect MPP2 in the precipitate (Fig 4a), suggesting that $GABA_A$ α1 is indeed a new binding partner for MPP2. Moreover, our comparative pull-down experiments using GST-tagged SH3GK domains of MPP2 and PSD-95 validate our mass spectrometry data (Fig 3) and demonstrate that MPP2 – in contrast to PSD-95 – binds effectively to $GABA_A$ α1: while the MPP2 SH3-GK domain efficiently pulls out the endogenous $GABA_A$ α1 from crude synaptosome preparations, the PSD-95 SH3-GK domain does not (Fig 4b).

Fig 4: Validation of $GABA_A$ α1 as novel interaction partner of MPP2.

(a) Untagged $GABA_A$ α1 was overexpressed in CHL V79 cells together with FLAG-tagged MPP2 and subjected to pull-down with α$GABA_A$ α1 or normal Ms IgG. Co-purification of FLAG-MPP2 was detected by Western blot with αFLAG and α$GABA_A$ α1 primary and α-native-Ms-IgG (Veriblot) secondary antibodies. Asterisk (*) marks re-emergence of αFLAG-HRP signal from the previous exposure.

(b) Bacterially expressed GST-MPP2-SH3GK and GST-PSD-95-SH3GK were incubated with crude brain synaptosome preparations. After GST pull-down, compared to bead control, $GABA_A$ α1 was efficiently enriched in the GST-MPP2-SH3GK pull-down, as detected by western blot with α$GABA_A$ α1 and αGST antibodies.

MPP2 co-localises with endogenous $GABA_A$ α1 in a sub-population of dendritic spines

Our *in vitro* experiments clearly show that $GABA_A$ receptor α1 subunits preferentially interact with the C-terminal SH3GK module of MPP2. In light of the fact that $GABA_A$ receptors are best known for their importance at inhibitory synapses where Gephyrin is the predominant scaffold (for review see [33]), this result was surprising. To explore the idea that $GABA_A$ receptors interact with MPP2 at glutamatergic synapses, we immunostained dissociated rat primary hippocampal neurons for the endogenous proteins. Neuronal cultures were fixed at DIV21 and stained for $GABA_A$ α1 and MPP2 together with the dendritic marker MAP2 (microtubule-associated protein 2) and the postsynaptic density marker Homer1, with respective primary and secondary antibodies. MPP2 (Fig 5, cyan) is present in almost all dendritic spines positive for the PSD marker Homer1 (Fig 5, yellow). Upon analysis of secondary dendrites (Fig 5b), we observed $GABA_A$ α1 signals (Fig 5, magenta) not only along MAP2-positive dendritic branches, where expected (Fig 5, blue), but also co-localising directly with MPP2 and Homer1 in a subset of dendritic spines (Fig 5b and c). More detailed examination of selected spines via line plot analysis of fluorescence intensity (Fig 5d) confirmed three different patterns of protein expression among the spines in our cultures: synapses positive for all three proteins of interest (Fig 5d i), excitatory synapses positive for MPP2 and Homer1 (Fig 5d ii), and inhibitory synapses at the dendrite expressing $GABA_A$ α1 but negative for MPP2 and Homer1 (Fig 5d iii).

Fig 5: $GABA_A$ receptor subunits α1 co-localise with MPP2 in a subset of dendritic spines.

(a) Primary E18 rat hippocampal neurons were fixed at DIV21 and immunostained for endogenous proteins MAP2 (microtubule-associated protein 2), MPP2, $GABA_A$ α1 and Homer1 using respective primary and Alexa fluorophore-coupled secondary antibodies, and visualised by confocal microscopy. Box in this single-plane overview indicates location of detail image in b.

(b) Maximum projection composite of four-colour confocal immunofluorescence images acquired with 5x zoom depicts primary and secondary dendrite branches of a mature (DIV21) hippocampal neuron. Arrows indicate several dendritic spines where $GABA_A$ α1 co-localises with Homer1 and MPP2. Box indicates further zoom in c.

(c) Detail zoom of a secondary dendrite branch. Markers at positions a, b and c indicate line plot measurement locations shown in d.

(d) Normalised fluorescence intensity line plot quantification of exemplary dendritic spines as shown in c. Along the dendrite we find synapses in which $GABA_A$ α1, Homer1 and MPP2 clearly co-localise (i) and synapses positive for Homer1 and MPP2 with no $GABA_A$ α1 immunofluorescence (ii), as well as solely $GABA_A$ α1 positive punctae, likely representing inhibitory synapses at the dendrite (iii).

Together with our *in vitro* data, these results suggest that MPP2 and $GABA_A$ receptors interact in a sub-population of excitatory synapses and that MPP2 acts as a scaffold protein potentially involved in the recruitment and anchoring of $GABA_A$ receptors at these synapses.

Discussion

We are interested in how sub-synaptic nanodomains at glutamatergic synapses are organised such that they can orchestrate synaptic function, which is highly dynamic. Here we show that PSD-95 and MPP2, two related synaptic MAGUKs, are close, but distinctly localised at the PSD of glutamatergic synapses. Using super-resolution imaging strategies, we observe that SynCAM1 and MPP2 are located in juxtapose association towards the outside of the PSD, with both proteins surrounding central PSD-95 protein complexes at radial distances that reflect a peripheral PSD localisation, given typical expected PSD sizes [19].

These observations, combined with the fact that MPP2 interacts directly with the peripheral SynCAM1 (but not the more central AMPAR-auxiliary subunits, TARPs), led us to pursue the idea that MPP2 may act as a scaffold for protein complexes that are distinct from those at the core of the PSD. Using a comparative mass spectrometry approach, we demonstrate here that the SH3GK domains of MPP2 and PSD-95, which are structurally similar, indeed interact with distinct sets of cytosolic and membrane proteins present within dendritic spines. Importantly, we identified several novel MPP2-interacting proteins, including multiple $GABA_A$ receptor subunits as well as signalling molecules with established roles in the regulation of inhibitory transmission. Moreover, in hippocampal neuronal cultures, we observe a subset of glutamatergic synapses that clearly express both $GABA_A$ receptors and MPP2. Together, these data indicate a role for MPP2 as a scaffold protein that organises sub-synaptic nanodomains distinct from those defined by PSD-95, and highlight its potential to act as a mediator of inhibitory signalling at glutamatergic synapses.

Our combined imaging strategies illustrate that MPP2 and SynCAM1 sit directly next to each other towards the outside of the PSD, positioned optimally to regulate the formation of peripheral sub-synaptic nanodomains, and our comparative quantitative mass spectrometry data provide further information on the nature of these protein complexes. Importantly, well-known PSD-95-interacting proteins, including e.g. Map1a and MecP2, were highly enriched in the PSD-95-SH3GK pull-downs, whereas Farp1, a well-characterised SynCAM1 interactor and modulator of SynCAM-mediated processes [34], was found to be significantly enriched in our MPP2-SH3GK pull-downs. These data in particular illustrate the utility of our strategy for identifying unknown MPP2 interactors of potential importance.

Among the crude synaptosome proteins present in the MPP2-SH3GK pull-down, we consistently identified seven $GABA_A$ receptor subunits, i.e. more than one-third of all known subunits[35]. The fact that so many $GABA_A$ receptor subunits were in the top hits among MPP2-associated peptides supports the idea that the MAGUK-$GABA_A$ receptor association is MPP-specific and that these receptors do not generally bind with high affinity to the SH3GK domains of other synaptic MAGUKs. In co-immunoprecipitation experiments we could confirm a direct interaction of $GABA_A$ α1 with MPP2. Moreover, in our primary hippocampal neuron cultures, we also detect endogenous $GABA_A$ receptors in a subset of Homer1-positive glutamatergic synapses that express MPP2, providing support for the idea that there may be a functional role of MPP2-$GABA_A$ receptor protein complexes in dendritic spines.

$GABA_A$ receptors mediate inhibitory transmission onto dendrites at diverse locations of the dendritic arbour (for reviews see [32, 33, 36]). Detailed studies on their cellular localisation have revealed that $GABA_A$ receptor complexes are present not only on dendritic shafts but also in dendritic spines and in close proximity to PSDs of glutamatergic synapses [37]. Using electron microscopy, this perisynaptic localisation of $GABA_A$ receptor subunits has also been monitored by other groups in a developmental context [38], and more recently, the importance of $GABA_A$ receptors within dendritic spines and their role in regulating Ca^{2+} influx [39] and general excitatory signal transmission [40] has become a topic of

considerable interest (for review see [36]). Recent studies also highlight that $GABA_A$ receptor mobility between inhibitory synapses is an important mechanism by which inhibitory synaptic currents are regulated, and that this process can be modulated by activation of ionotropic glutamate receptors and subsequent trapping of desensitized $GABA_A$ receptors at glutamatergic synapses [41]. Clearly, there are multiple functional links between $GABA_A$ receptor signals and glutamatergic transmission at the PSD. However, the physical interactions that enable these connections have not been investigated to date. Our imaging studies highlight that MPP2 is positioned optimally – next to the core components of glutamate receptor signalling complexes, but at the periphery of the PSD – to play a structural role in orchestrating the complex formation that would be required to enable these dynamic links between glutamatergic transmission and $GABA_A$ receptor signalling.

We have previously demonstrated that MPP2 is linked to AMPA receptor protein complexes via SH3GK domain-mediated interactions with the core AMPA receptor-associated scaffold proteins PSD-95 and GKAP. Here we show that the same domains are responsible for specific interactions with $GABA_A$ receptors. Interestingly, the L27 domains at the N-terminus of MPP2 molecules are well known for their role in mediating MPP2 dimerisation [42]. In this context, our data, which demonstrates a physical link between $GABA_A$ receptors and MPP2 at glutamatergic synapses, lead us to propose a model in which MPP2 multi-molecular complexes serve as adaptors that enable crosstalk between $GABA_A$ receptor-mediated inhibitory regulation and glutamatergic transmission in dendritic spines (see Fig 6). Our model is further supported by the fact that one of the other novel MPP2 interaction partners identified in this study has previously been associated with inhibitory signalling through $GABA_A$ receptors: the calcium- and calmodulin-dependent serine/threonine protein phosphatase (Calcineurin) subunit Ppp3ca directly interacts with $GABA_A$ receptors [43-45].

In summary, our study provides insights into the physical interactions that mediate complex formation in dendritic spines. We demonstrate that the MPP2 scaffold protein serves to link core proteins of glutamatergic synapses with $GABA_A$ receptors and associated signalling molecules in dendritic spines,

and thereby illuminate its potential to facilitate crosstalk between excitatory and inhibitory transmission at the PSD of glutamatergic synapses.

Fig 6: Schematic summary of novel MPP2 interactors.

Our data indicate an important role of MPP2 (blue) in the sub-synaptic compartmentalisation of dendritic spines by connecting central components of AMPA receptor (orange) complexes, like TARPs (yellow) and PSD-95 (grey) not only to cell adhesion proteins like SynCAM (magenta) and other scaffold and regulatory proteins (like the novel interaction partners PIP5k1c or Ppp3ca), but most importantly inhibitory $GABA_A$ receptors (green). For MAGUK proteins the individual domain structure is indicated.

Materials and Methods

Primary neuronal cultures

Primary hippocampal neurons were prepared as described before [13] with protocols approved by 'Landesamt für Gesundheit und Soziales' (LaGeSo; Regional Office for Health and Social Affairs; permit number T0280/10) in Berlin. Briefly, E18 Wistar rat pups were decapitated, hippocampi isolated and digested with Trypsin/EDTA (Lonza). Digest was stopped with DMEM/10 % FBS (Biochrom), followed by washing in DMEM (Lonza). Tissue was then dissociated and plated at ~10^5 cells per cm² in neuron culture medium (Neurobasal (Lifetech) supplemented with B27 (Gibco) and 500 µM L-glutamine (Lonza)) onto coverslips coated with poly-D-Lysine (0,2 mg/ml, Sigma) and Laminin (2 µg/ml, Sigma) and maintained in a humidified incubator (37°C, 5% CO_2).

Immunocytochemistry/Immunofluorescence

Primary rat hippocampal neurons were fixed at DIV21 with 4 % PFA/PBS for 10 min at RT, washed thrice for 10 min with PBS, followed by 45 min quenching at RT with 50 mM NH_4Cl to reduce auto-fluorescence. After washing with PBS, cells were permeabilised with 0.2 % Triton-X/PBS for 5 min and washed with PBS. For dSTORM microscopy cells were additionally treated with Image-IT Signal Enhancer (Thermo Fisher) for 30 min at RT and three washes with PBS. Cells were then blocked for at least 1 hr at RT with blocking solution (4% BSA/PBST). Primary antibodies were diluted 1:250 in blocking solution (1:500 for confocal microscopy) and incubated over night at 4°C, followed by incubation with desired secondary antibodies at 1:1000 dilution in blocking solution for 1 hr at RT and for *d*STORM custom-labelled secondary antibodies at 1 µg/ml (~7 nM) in blocking solution for 20 min, followed by post-fixation and quenching as above. After final washing with PBS, coverslips were mounted with Fluoromount G (SBA) or Vectashield (H1000, Vector Laboratories) for confocal and SIM imaging, respectively.

Primary antibodies: αMPP2 (rabbit, ab97290, Abcam), αMAP2 (guinea pig, 188004, Synaptic Systems), αPSD-95 (mouse, 75-028, NeuroMab), αvGlut1 (guinea pig, 135 304, Synaptic Systems), αGABA$_A$ α1 (mouse, 75-136, NeuroMab), αSynCAM (chicken, CM004-3, MBL), GFP-Booster (nanobody, gba488-10, Chromotek)

Secondary antibodies: αMouse Alexa Fluor 405 (A-31553, Invitrogen), αGuinea pig Alexa Fluor 405 (ab175678, Abcam), αGuinea pig DyLight405 (706-475-148, Dainova), αRabbit Alexa Fluor 488 (A-21441, Invitrogen), αChicken Alexa Fluor 488 (703-545-155, Jackson Immuno Research), αMouse Alexa Fluor 568 (A-11031, Life Technologies), αRabbit Alexa Fluor 568 (A-11036, Invitrogen), αRabbit

(111-005-003, AffiniPure), αMouse (715-005-151, AffiniPure), αMouse Alexa Fluor 647 (715-605-150, Jackson Immuno Research), αChicken Alexa Fluor 647 (103-605-155, Dianova).

Confocal Microscopy

Cells were fixed and stained as described above and imaged with a Leica TCS SP5 II confocal laser scanning microscope run with LAS AF X scan software (Leica Microsystems, Wetzlar, Germany). Image stacks were acquired with a 63x oil immersion objective at 2x zoom for overviews and 5x zoom for details at 2048x2048 px as 5-7 planes with 0.4 µm step size in Z. Image analysis was performed in Fiji/ImageJ[46, 47]. The three highest intensity planes for Homer1 were selected and maximum projected. Then, line plot profile measurements were taken for individual spines for every channel. Data was then 0/1 normalised across all acquired values within one channel.

Dual-colour *d*STORM imaging

Labelling of antibodies: Secondary antibodies (goat αRabbit, 111-005-003, AffiniPure or donkey αMouse, 715-005-151, AffiniPure) were diluted 1:10 in labelling buffer (0.2 M $NaHCO_3$, pH 8.3). Cy3b NHS Ester (PA63101, Life Sciences) was added to the diluted antibodies in 10-fold molar excess. The samples were incubated for 1 hr at room temperature. To stop the reaction, 100 mM Tris pH 8.0 was added. Zebra spin desalting columns (8989, Thermofisher) were equilibrated with PBS. The samples were added to the column and centrifuged at 1000 *g* for 2 min. The filtrate was added to a second column and centrifuged at 1000 *g* for 2 min.

Image acquisition: All samples were imaged using a Vutara 352 super-resolution microscope (Bruker) equipped with a Hamamatsu ORCA Flash4.0 sCMOS camera for super-resolution imaging and a 60x oil immersion TIRF objective with a numerical aperture of 1.49 (Olympus). Immersion Oil 23°C (#1261, Cargille) was used. Samples were mounted onto the microscope in GLOX buffer (1.5% β-mercaptoethanol, 0.5% (v/w) glucose, 0.25 mg/ml glucose oxidase and 20 µg/ml catalase, 150 mM Tris-HCl pH 8.8), illumination at a laser-power density of 5.5 kW/cm2 using a 637 nm laser for Alexa Fluor 647 or a 561 nm laser at a laser-power density of 4.6 kW/cm² for Cy3b. Images were collected with 20 ms acquisition time. Per probe (Cy3b or Alexa Fluor 647) 10,000 frames were acquired. Acquired raw data were localized using SRX (Bruker). Localisations were filtered according to Thompsom accuracy [18], i.e. all localisations with accuracy worse than 20 nm were excluded. Localisations were rendered as Gaussian distributions with a constant width of 20 nm. Alignment of

colour channels and drift correction were performed in SRX using Tetraspeck beads (Thermofisher, T7279). Supplemental Figures 1-3 were prepared using the ScientiFig Plugin for Fiji/ImageJ [48].

Structured Illumination Microscopy

Sample preparation: Primary hippocampal rat neurons (DIV21) stained for the presynaptic marker vGlut1 and the postsynaptic proteins PSD-95, SynCAM1 and MPP2 as described above.

Image acquisition: Targets were selected based on the SynCAM1 signal. Three-dimensional SIM images were acquired with the OMX V4 Blaze system (GE Healthcare), using the 405 nm, 488 nm, 568 nm and 647 nm laser lines, a 60x 1.42 N.A. oil objective (Olympus), an immersion oil with a refractive index of 1.518 and standard emission filters at 125 nm z-sectioning. Multi-colour registration with an error below 40 nm was done using 100 nm fluorescent beads (TetraSpeck, T7284, Thermo Fisher Scientific). Images were acquired with the DeltaVision OMX acquisition software (GE Healthcare) and images were reconstructed with softWoRx (GE Healthcare).

SIM Image Analysis

Segmentation: Image segmentation was performed in Arivis Vision 4D (Arivis AG, Munich, Germany). MPP2, SynCAM1 and vGlut1 clusters were identified with histogram-based threshold procedures (Otsu's and Yen's method). PSD 95 clusters and their centres were identified with the built in "Blob Finder" tool, a combination of automatic seed finding and watershed segmentationand further filtered for sphericity (> 0.4), volume (> 000.5 μm^3) and co-existence of MPP2-, SynCAM1- and vGlut1 staining within the same synapse (2.5 µm distance cut-off to the centre of the next PSD-95 cluster). M

Radial intensity profiles: A custom-written ImageJ [46] script (https://github.com/ngimber/RadialProfile3D) was used to calculate 3D radial intensity profiles around PSD-95 centres (segmentation from above). Radial intensity profiles were summarized, 0-1 normalised and averaged twice (per image and per experiment) using Python before plotting with Prism 7 (GraphPad).

Nearest neighbour analysis: Nearest neighbour analysis and randomizations were performed in Python using custom-written scripts. Nearest neighbour distances between PSD-95, MPP2 and SynCAM1 cluster were calculated based on the Arivis segmentations. Random controls were generated by randomly distributing spherical objects, representing PSD-95, MPP2 and SynCAM1 clusters within a simplified spherical post-synapse with a diameter of 0.8 µm[19]. Randomised distributions were

463 generated for each image using the object counts and volumes from the corresponding segmentation
464 (10 simulation rounds per synapse, ~ 40.000 synapses from 50 images). Plotting was done with Prism 7
465 (GraphPad).

466 *Object statistics:* Object counts and sizes were obtained from the segmentation above (Arivis).
467 Histograms (bin size = 15 nm) from cluster sizes were plotted in R+.

468

469 **Cell culture and transfection**

470 HEK293T and CHL V79 cells were maintained in low-glucose DMEM supplemented with 10% FCS,
471 1000 U/ml penicillin/streptomycin and 2 mM L-glutamine in a humidified incubator at 37 °C with 5%
472 CO_2. Transfections were performed using Lipofectamine 2000 (Invitrogen) and desired DNA constructs
473 diluted in Opti-MEM (Gibco).

474

475 **DNA constructs**

476 N-terminal FLAG-tagged MPP2 and PSD-95 were cloned as described before [13, 49]. Full length mouse
477 MPP2 (NM_016695) was cloned into pEGFP-C1, to obtain N-terminal EGFP-tagged EGFP-MPP2. Full-
478 length rat SynCAM1 (NM_001012201.1) was synthesised as described before [13]. Clover-PSD-95.
479 Expression constructs for Flag-tagged full-length rat proteins were generated by cloning Arhgef2
480 (NM_001012079), Ppp3ca (NM_017041) and Farp1 (NM_001107287) into pCMV-Tag 2A. HA-Gnao1
481 (NM_017327) was constructed by PCR with a forward primer that encodes the HA tag and cloned with
482 NotI and SalI into pCMV-Tag 2A.

483 GFP-PIPK1 gamma 90 was a gift from Pietro De Camilli (Addgene plasmid # 22299;
484 http://n2t.net/addgene:22299; RRID: Addgene_22299). GABA (A) receptor subunit a1SE was a gift
485 from Tija Jacob & Stephen Moss (Addgene plasmid # 49168; http://n2t.net/addgene:49168; RRID:
486 Addgene_49168). Rat $GABA_A\alpha1$ (NM_183326) was cloned into pCMV-2A with NotI and SalI to generate
487 an untagged expression construct.

488 The bacterial expression construct GST-MPP2-SH3-GK was generated by cloning the fragment
489 encoding amino acids 220-552 (SH3GK) of mouse MPP2 into pGEX-6P-1 (GE Healthcare). GST-PSD-95-
490 SH3GK was generated as described before [25]. A fragment corresponding to amino acids 403-724 of
491 PSD-95 was cloned into pGEX-6P-1.

492

493

Co-immunoprecipitation

HEK293T cells were harvested 18-20 hrs after transfection with a cell scraper and cell lysates obtained with 30 gauge syringe needle strikes in immunoprecipitation buffer (50 mM Tris pH 7,4; 100 mM NaCl; 1 mM EDTA, 1% Triton-X or 0.1% NP-40; supplemented with Complete Mini protease inhibitors, Roche). Cell lysates were cleared by centrifugation (3x 10 min at 20000 *g* at 4°C) and supernatants were incubated with 2 µg αGFP (mouse, 75-131, NeuroMab), αGABA-Aα1 (mouse, 75-136, NeuroMab) or normal mouse IgG, respectively, for 3 hrs on a rotator (10 rpm) at 4°C. Pull-down was performed with 30 µl protein-G-agarose bead slurry (Roche) for 1 hr at 4°C under gentle agitation, followed by three washes with IP buffer and final analysis by western blot.

Western Blotting

Lysates and beads were boiled in 2x SDS-sample buffer (8% SDS, 40% glycerol, 0,25 M Tris pH 6.8, 20% β-mercaptoethanol) for 5 min, separated on a 10% SDS-PAGE and blotted onto PVDF membranes (Roche). Membranes were blocked with 5% skim milk/PBST. Primary antibodies were diluted in the blocking buffer and applied over night at 4°C, followed by three washes with PBST and 1 hr incubation with appropriate secondary antibodies. HRP-signals were detected using Western Lightning chemiluminescent substrates (Perkin Elmer) with a luminescent image analyser (ImageQuant LAS4000, GE Healthcare).

Primary antibodies: αSynCAM (rabbit, PA3-16744, Thermo Scientific), αMPP2 (rabbit, ab97290, Abcam), αPSD-95 (mouse, 75-028, NeuroMab), αGABA$_A$ α1 (mouse, 75-136, NeuroMab), αFlag (mouse, F1804, Sigma), αFlag-HRP (mouse, A8592, Sigma), αGFP (chicken, ab13970, Abcam), αGST (mouse, 75-148, NeuroMab).

Secondary antibodies: αMouse-HRP (115-035-003, Dianova), αMouse-native-IgG (Veriblot, 131368, Abcam), αRabbit-HRP (111-035-003, Dianova), αRat-HRP (sc-2032, Santa Cruz), αChicken-HRP (ab6753, Abcam).

Crude synaptosome fraction preparation

For immunoprecipitation using brain lysates, adult Wistar rats were administered isofluorane anaesthesia prior to decapitation and reported under permit T0280/10 (LaGeSO). The brains were removed and rinsed in ice-cold PBS. Brains were immediately frozen and stored at -80°C until use. Brains (~2 g) were then thawed on ice, minced with a scalpel and homogenized in 20 ml Syn-PER

Synaptic Protein Extraction Reagent (Thermo Science) according to the manufacturer's protocol. For co-immunoprecipitation, the resulting crude synaptosome fraction was then resuspended in IP buffer (50 mM Tris pH 7,4; 100 mM NaCl; 1 mM EDTA, 1% Triton-X; supplemented with Complete Mini protease inhibitors, Roche) and cleared by 3x centrifugation at 20000 *g*. For GST pull-down, the pellet was solubilised in 10 ml 1% Triton-X/PBS.

GST pull-down

GST-SH3-GK domain constructs of PSD-95 and MPP2 were expressed in *E.coli* BL21 DE3 and purified according to the manufacturer's manual (GST Gene Fusion System, GE Healthcare). 30 µl of glutathione agarose (Pierce) was loaded with GST-SH3-GK proteins (PSD-95 and MPP2) and incubated for 3 hrs with protein lysate from crude synaptosomes. The beads were washed three times with PBS/1% Triton X-100 and eluted from the matrix by incubation with SDS sample buffer for 5 min at 95°C.

Sample preparation and liquid chromatography-mass spectrometry (LC-MS)

Proteins from two technical replicates were separated by SDS-PAGE (10% Tricine-SDS-PAGE). Coomassie-stained lanes were cut into 12 slices and in-gel protein digestion and $^{16}O/^{18}O$-labelling was performed as described previously [50, 51]. In brief, corresponding samples (PSD-95 and MPP2) were incubated overnight at 37°C with 50 ng trypsin (sequencing grade modified, Promega) in 25 µl of 50 mM ammonium bicarbonate in the presence of heavy water (Campro Scientific GmbH, 97% ^{18}O) and regular ^{16}O-water, respectively. Isotope-labels were switched between the two replicates. To prevent oxygen back-exchange by residual trypsin activity, samples were heated at 95°C for 20 min. After cooling down, 50 µl of 0.5% trifluoroacetic acid (TFA) in acetonitrile was added to decrease the pH of the sample from pH8 to pH2. Afterwards, corresponding heavy- and light-isotope labelled samples were combined and peptides were dried under vacuum. Peptides were reconstituted in 10 µl of 0.05% TFA, 2% acetonitrile, and 6.5 µl were analysed by a reversed-phase nano liquid chromatography system (Ultimate 3000, Thermo Scientific) connected to an Orbitrap Velos mass spectrometer (Thermo Scientific). Samples were injected and concentrated on a trap column (PepMap100 C18, 3 µm, 100 Å, 75 µm i.d. x 2 cm, Thermo Scientific) equilibrated with 0.05% TFA, 2% acetonitrile in water. After switching the trap column inline, LC separations were performed on a capillary column (Acclaim PepMap100 C18, 2 µm, 100 Å, 75 µm i.d. x 25 cm, Thermo Scientific) at an eluent flow rate of 300 nl/min. Mobile phase A contained 0.1% formic acid in water, and mobile phase B contained 0.1% formic acid in acetonitrile. The column was pre-equilibrated with 3% mobile phase B followed by an increase of 3–50% mobile phase B in 50 min. Mass spectra were acquired in a data-dependent mode using a

558 single MS survey scan (m/z 350–1500) with a resolution of 60,000 in the Orbitrap, and MS/MS scans
559 of the 20 most intense precursor ions in the linear trap quadrupole. The dynamic exclusion time was
560 set to 60 s and automatic gain control was set to 1 x 10^6 and 5,000 for Orbitrap-MS and LTQ-MS/MS
561 scans, respectively.
562

563 **Proteomic data analysis**

564 Identification and quantification of $^{16}O/^{18}O$-labelled samples was performed using the Mascot Distiller
565 Quantitation Toolbox (version 2.7.1.0, Matrix Science). Data were compared to the SwissProt protein
566 database using the taxonomy rattus (August 2017 release with 7996 protein sequences) including the
567 sequences of the employed protein constructs and the sequence of the GST tag. A maximum of two
568 missed cleavages was allowed and the mass tolerance of precursor and sequence ions was set to 15
569 ppm and 0.35 Da, respectively. Methionine oxidation, acetylation (protein N-terminus), propionamide
570 (Cysteine), and C-terminal $^{18}O_1$- and $^{18}O_2$-isotope labelling were used as variable modifications. A
571 significance threshold of 0.05 was used based on decoy database searches. For quantification at
572 protein level, a minimum of two quantified peptides was set as a threshold. Protein ratios were
573 calculated from the intensity-weighted average of all corresponding peptide ratios. The protein ratio
574 of GST was used for normalisation of protein ratios. Only proteins that were quantified in both
575 replicates with a standard deviation of <2 were considered. Known contaminants (e.g. keratins) and
576 the bait proteins were removed from the protein output table.
577

578

579 ## Acknowledgements

We are grateful for technical assistance from Melanie Fuchs. For mass spectrometry, we would like to acknowledge the assistance of the Core Facility BioSupraMol.

580

581 # References
582

583 1. Elias GM, Funke L, Stein V, Grant SG, Bredt DS, Nicoll RA. Synapse-specific and developmentally
584 regulated targeting of AMPA receptors by a family of MAGUK scaffolding proteins. Neuron.
585 2006;52(2):307-20. doi: 10.1016/j.neuron.2006.09.012. PubMed PMID: 17046693.
586 2. Sheng M, Hoogenraad CC. The postsynaptic architecture of excitatory synapses: a more
587 quantitative view. Annual review of biochemistry. 2007;76:823-47. Epub 2007/01/25. doi:
588 10.1146/annurev.biochem.76.060805.160029. PubMed PMID: 17243894.
589 3. Won S, Levy JM, Nicoll RA, Roche KW. MAGUKs: multifaceted synaptic organizers. Curr Opin
590 Neurobiol. 2017;43:94-101. Epub 2017/02/27. doi: 10.1016/j.conb.2017.01.006. PubMed
591 PMID: 28236779; PubMed Central PMCID: PMCPMC5447471.
592 4. Dani A, Huang B, Bergan J, Dulac C, Zhuang X. Superresolution imaging of chemical synapses in
593 the brain. Neuron. 2010;68(5):843-56. Epub 2010/12/15. doi: 10.1016/j.neuron.2010.11.021.
594 PubMed PMID: 21144999; PubMed Central PMCID: PMCPMC3057101.
595 5. MacGillavry HD, Song Y, Raghavachari S, Blanpied TA. Nanoscale scaffolding domains within the
596 postsynaptic density concentrate synaptic AMPA receptors. Neuron. 2013;78(4):615-22. Epub
597 2013/05/31. doi: 10.1016/j.neuron.2013.03.009. PubMed PMID: 23719161; PubMed Central
598 PMCID: PMCPMC3668352.
599 6. Nair D, Hosy E, Petersen JD, Constals A, Giannone G, Choquet D, et al. Super-resolution imaging
600 reveals that AMPA receptors inside synapses are dynamically organized in nanodomains
601 regulated by PSD95. J Neurosci. 2013;33(32):13204-24. Epub 2013/08/09. doi:
602 10.1523/JNEUROSCI.2381-12.2013. PubMed PMID: 23926273.
603 7. Biederer T, Kaeser PS, Blanpied TA. Transcellular Nanoalignment of Synaptic Function. Neuron.
604 2017;96(3):680-96. doi: 10.1016/j.neuron.2017.10.006. PubMed PMID: 29096080; PubMed
605 Central PMCID: PMCPMC5777221.
606 8. MacGillavry HD, Kerr JM, Blanpied TA. Lateral organization of the postsynaptic density. Mol Cell
607 Neurosci. 2011;48(4):321-31. Epub 2011/09/17. doi: 10.1016/j.mcn.2011.09.001. PubMed
608 PMID: 21920440; PubMed Central PMCID: PMCPMC3216044.
609 9. Yang X, Specht CG. Subsynaptic Domains in Super-Resolution Microscopy: The Treachery of
610 Images. Front Mol Neurosci. 2019;12:161. Epub 2019/07/18. doi: 10.3389/fnmol.2019.00161.
611 PubMed PMID: 31312120; PubMed Central PMCID: PMCPMC6614521.
612 10. Wegner W, Mott AC, Grant SGN, Steffens H, Willig KI. In vivo STED microscopy visualizes PSD95
613 sub-structures and morphological changes over several hours in the mouse visual cortex. Sci
614 Rep. 2018;8(1):219. Epub 2018/01/11. doi: 10.1038/s41598-017-18640-z. PubMed PMID:
615 29317733; PubMed Central PMCID: PMCPMC5760696.
616 11. Choquet D, Triller A. The dynamic synapse. Neuron. 2013;80(3):691-703. Epub 2013/11/05. doi:
617 10.1016/j.neuron.2013.10.013. PubMed PMID: 24183020.
618 12. Kim G, Lujan R, Schwenk J, Kelley MH, Aguado C, Watanabe M, et al. Membrane palmitoylated
619 protein 2 is a synaptic scaffold protein required for synaptic SK2-containing channel function.
620 Elife. 2016;5. doi: 10.7554/eLife.12637. PubMed PMID: 26880549.
621 13. Rademacher N, Schmerl B, Lardong JA, Wahl MC, Shoichet SA. MPP2 is a postsynaptic MAGUK
622 scaffold protein that links SynCAM1 cell adhesion molecules to core components of the
623 postsynaptic density. Sci Rep. 2016;6:35283. doi: 10.1038/srep35283. PubMed PMID:
624 27756895; PubMed Central PMCID: PMCPMC5069480.
625 14. Schwenk J, Harmel N, Brechet A, Zolles G, Berkefeld H, Muller CS, et al. High-resolution proteomics
626 unravel architecture and molecular diversity of native AMPA receptor complexes. Neuron.
627 2012;74(4):621-33. doi: 10.1016/j.neuron.2012.03.034. PubMed PMID: 22632720.
628 15. Shanks NF, Savas JN, Maruo T, Cais O, Hirao A, Oe S, et al. Differences in AMPA and kainate
629 receptor interactomes facilitate identification of AMPA receptor auxiliary subunit GSG1L. Cell
630 reports. 2012;1(6):590-8. doi: 10.1016/j.celrep.2012.05.004. PubMed PMID: 22813734;
631 PubMed Central PMCID: PMC3401968.

16. de Arce KP, Schrod N, Metzbower SWR, Allgeyer E, Kong GKW, Tang AH, et al. Topographic Mapping of the Synaptic Cleft into Adhesive Nanodomains. Neuron. 2015;88(6):1165-72. doi: 10.1016/j.neuron.2015.11.011. PubMed PMID: WOS:000368443900013.
17. Perez de Arce K, Schrod N, Metzbower SW, Allgeyer E, Kong GK, Tang AH, et al. Topographic Mapping of the Synaptic Cleft into Adhesive Nanodomains. Neuron. 2015;88(6):1165-72. doi: 10.1016/j.neuron.2015.11.011. PubMed PMID: 26687224; PubMed Central PMCID: PMCPMC4687029.
18. Thompson RE, Larson DR, Webb WW. Precise Nanometer Localization Analysis for Individual Fluorescent Probes. Biophysical Journal. 2002;82(5):2775-83. doi: 10.1016/s0006-3495(02)75618-x.
19. Adrian M, Kusters R, Storm C, Hoogenraad CC, Kapitein LC. Probing the Interplay between Dendritic Spine Morphology and Membrane-Bound Diffusion. Biophys J. 2017;113(10):2261-70. Epub 2017/07/29. doi: 10.1016/j.bpj.2017.06.048. PubMed PMID: 28750887; PubMed Central PMCID: PMCPMC5700248.
20. Haas KT, Compans B, Letellier M, Bartol TM, Grillo-Bosch D, Sejnowski TJ, et al. Pre-post synaptic alignment through neuroligin-1 tunes synaptic transmission efficiency. Elife. 2018;7. Epub 2018/07/26. doi: 10.7554/eLife.31755. PubMed PMID: 30044218; PubMed Central PMCID: PMCPMC6070337.
21. Irie M, Hata Y, Takeuchi M, Ichtchenko K, Toyoda A, Hirao K, et al. Binding of neuroligins to PSD-95. Science. 1997;277(5331):1511-5. PubMed PMID: 9278515.
22. Kornau HC, Schenker LT, Kennedy MB, Seeburg PH. Domain interaction between NMDA receptor subunits and the postsynaptic density protein PSD-95. Science. 1995;269(5231):1737-40. Epub 1995/09/22. doi: 10.1126/science.7569905. PubMed PMID: 7569905.
23. Schnell E, Sizemore M, Karimzadegan S, Chen L, Bredt DS, Nicoll RA. Direct interactions between PSD-95 and stargazin control synaptic AMPA receptor number. Proc Natl Acad Sci U S A. 2002;99(21):13902-7. doi: 10.1073/pnas.172511199. PubMed PMID: 12359873; PubMed Central PMCID: PMCPMC129795.
24. Zhu J, Shang Y, Xia C, Wang W, Wen W, Zhang M. Guanylate kinase domains of the MAGUK family scaffold proteins as specific phospho-protein-binding modules. EMBO J. 2011;30(24):4986-97. doi: 10.1038/emboj.2011.428. PubMed PMID: 22117215; PubMed Central PMCID: PMCPMC3243629.
25. Rademacher N, Kuropka B, Kunde SA, Wahl MC, Freund C, Shoichet SA. Intramolecular domain dynamics regulate synaptic MAGUK protein interactions. Elife. 2019;8. Epub 2019/03/14. doi: 10.7554/eLife.41299. PubMed PMID: 30864948; PubMed Central PMCID: PMCPMC6438691.
26. Zeng M, Ye F, Xu J, Zhang M. PDZ Ligand Binding-Induced Conformational Coupling of the PDZ-SH3-GK Tandems in PSD-95 Family MAGUKs. J Mol Biol. 2018;430(1):69-86. Epub 2017/11/16. doi: 10.1016/j.jmb.2017.11.003. PubMed PMID: 29138001.
27. Bayes A, Collins MO, Croning MD, van de Lagemaat LN, Choudhary JS, Grant SG. Comparative study of human and mouse postsynaptic proteomes finds high compositional conservation and abundance differences for key synaptic proteins. PLoS One. 2012;7(10):e46683. Epub 2012/10/17. doi: 10.1371/journal.pone.0046683. PubMed PMID: 23071613; PubMed Central PMCID: PMCPMC3465276.
28. Danti FR, Galosi S, Romani M, Montomoli M, Carss KJ, Raymond FL, et al. GNAO1 encephalopathy: Broadening the phenotype and evaluating treatment and outcome. Neurol Genet. 2017;3(2):e143. Epub 2017/03/31. doi: 10.1212/NXG.0000000000000143. PubMed PMID: 28357411; PubMed Central PMCID: PMCPMC5362187.
29. Kang MG, Guo Y, Huganir RL. AMPA receptor and GEF-H1/Lfc complex regulates dendritic spine development through RhoA signaling cascade. Proc Natl Acad Sci U S A. 2009;106(9):3549-54. Epub 2009/02/12. doi: 10.1073/pnas.0812861106. PubMed PMID: 19208802; PubMed Central PMCID: PMCPMC2638734.
30. Barrera NP, Betts J, You H, Henderson RM, Martin IL, Dunn SM, et al. Atomic force microscopy reveals the stoichiometry and subunit arrangement of the alpha4beta3delta GABA(A)

receptor. Mol Pharmacol. 2008;73(3):960-7. Epub 2007/12/15. doi: 10.1124/mol.107.042481. PubMed PMID: 18079275.

31. Patel B, Mortensen M, Smart TG. Stoichiometry of delta subunit containing GABA(A) receptors. Br J Pharmacol. 2014;171(4):985-94. Epub 2013/11/12. doi: 10.1111/bph.12514. PubMed PMID: 24206220; PubMed Central PMCID: PMCPMC3925037.
32. Chiu CQ, Barberis A, Higley MJ. Preserving the balance: diverse forms of long-term GABAergic synaptic plasticity. Nat Rev Neurosci. 2019;20(5):272-81. Epub 2019/03/07. doi: 10.1038/s41583-019-0141-5. PubMed PMID: 30837689.
33. Tyagarajan SK, Fritschy JM. Gephyrin: a master regulator of neuronal function? Nat Rev Neurosci. 2014;15(3):141-56. Epub 2014/02/21. doi: 10.1038/nrn3670. PubMed PMID: 24552784.
34. Cheadle L, Biederer T. The novel synaptogenic protein Farp1 links postsynaptic cytoskeletal dynamics and transsynaptic organization. J Cell Biol. 2012;199(6):985-1001. doi: 10.1083/jcb.201205041. PubMed PMID: 23209303; PubMed Central PMCID: PMCPMC3518221.
35. Sigel E, Steinmann ME. Structure, function, and modulation of GABA(A) receptors. The Journal of biological chemistry. 2012;287(48):40224-31. Epub 2012/10/06. doi: 10.1074/jbc.R112.386664. PubMed PMID: 23038269; PubMed Central PMCID: PMCPMC3504738.
36. Boivin JR, Nedivi E. Functional implications of inhibitory synapse placement on signal processing in pyramidal neuron dendrites. Curr Opin Neurobiol. 2018;51:16-22. Epub 2018/02/20. doi: 10.1016/j.conb.2018.01.013. PubMed PMID: 29454834; PubMed Central PMCID: PMCPMC6066407.
37. Kubota Y, Hatada S, Kondo S, Karube F, Kawaguchi Y. Neocortical inhibitory terminals innervate dendritic spines targeted by thalamocortical afferents. J Neurosci. 2007;27(5):1139-50. Epub 2007/02/03. doi: 10.1523/JNEUROSCI.3846-06.2007. PubMed PMID: 17267569; PubMed Central PMCID: PMCPMC6673192.
38. Shen H, Sabaliauskas N, Sherpa A, Fenton AA, Stelzer A, Aoki C, et al. A critical role for alpha4betadelta GABAA receptors in shaping learning deficits at puberty in mice. Science. 2010;327(5972):1515-8. Epub 2010/03/20. doi: 10.1126/science.1184245. PubMed PMID: 20299596; PubMed Central PMCID: PMCPMC2887350.
39. Marlin JJ, Carter AG. GABA-A receptor inhibition of local calcium signaling in spines and dendrites. J Neurosci. 2014;34(48):15898-911. Epub 2014/11/28. doi: 10.1523/JNEUROSCI.0869-13.2014. PubMed PMID: 25429132; PubMed Central PMCID: PMCPMC4244464.
40. Chen JL, Villa KL, Cha JW, So PT, Kubota Y, Nedivi E. Clustered dynamics of inhibitory synapses and dendritic spines in the adult neocortex. Neuron. 2012;74(2):361-73. Epub 2012/05/01. doi: 10.1016/j.neuron.2012.02.030. PubMed PMID: 22542188; PubMed Central PMCID: PMCPMC3340582.
41. de Luca E, Ravasenga T, Petrini EM, Polenghi A, Nieus T, Guazzi S, et al. Inter-Synaptic Lateral Diffusion of GABAA Receptors Shapes Inhibitory Synaptic Currents. Neuron. 2017;95(1):63-9.e5. doi: 10.1016/j.neuron.2017.06.022.
42. Li Y, Karnak D, Demeler B, Margolis B, Lavie A. Structural basis for L27 domain-mediated assembly of signaling and cell polarity complexes. EMBO J. 2004;23(14):2723-33. doi: 10.1038/sj.emboj.7600294. PubMed PMID: 15241471; PubMed Central PMCID: PMC514954.
43. Bannai H, Levi S, Schweizer C, Inoue T, Launey T, Racine V, et al. Activity-dependent tuning of inhibitory neurotransmission based on GABAAR diffusion dynamics. Neuron. 2009;62(5):670-82. Epub 2009/06/16. doi: 10.1016/j.neuron.2009.04.023. PubMed PMID: 19524526.
44. Bannai H, Niwa F, Sherwood MW, Shrivastava AN, Arizono M, Miyamoto A, et al. Bidirectional Control of Synaptic GABAAR Clustering by Glutamate and Calcium. Cell reports. 2015;13(12):2768-80. Epub 2015/12/30. doi: 10.1016/j.celrep.2015.12.002. PubMed PMID: 26711343; PubMed Central PMCID: PMCPMC4700050.
45. Wang J, Liu S, Haditsch U, Tu W, Cochrane K, Ahmadian G, et al. Interaction of Calcineurin and Type-A GABA Receptor γ2Subunits Produces Long-Term Depression at CA1 Inhibitory

Synapses. The Journal of Neuroscience. 2003;23(3):826-36. doi: 10.1523/jneurosci.23-03-00826.2003.

46. Schindelin J, Arganda-Carreras I, Frise E, Kaynig V, Longair M, Pietzsch T, et al. Fiji: an open-source platform for biological-image analysis. Nat Methods. 2012;9(7):676-82. Epub 2012/06/30. doi: 10.1038/nmeth.2019. PubMed PMID: 22743772; PubMed Central PMCID: PMCPMC3855844.
47. Schneider CA, Rasband WS, Eliceiri KW. NIH Image to ImageJ: 25 years of image analysis. Nat Methods. 2012;9(7):671-5. Epub 2012/08/30. doi: 10.1038/nmeth.2089. PubMed PMID: 22930834; PubMed Central PMCID: PMCPMC5554542.
48. Aigouy B, Mirouse V. ScientiFig: a tool to build publication-ready scientific figures. Nat Methods. 2013;10(11):1048. Epub 2013/11/01. doi: 10.1038/nmeth.2692. PubMed PMID: 24173380.
49. Rademacher N, Kunde SA, Kalscheuer VM, Shoichet SA. Synaptic MAGUK multimer formation is mediated by PDZ domains and promoted by ligand binding. Chemistry & biology. 2013;20(8):1044-54. doi: 10.1016/j.chembiol.2013.06.016. PubMed PMID: 23973190.
50. Kristiansen TZ, Harsha HC, Grønborg M, Maitra A, Pandey A. Differential Membrane Proteomics Using18O-Labeling To Identify Biomarkers for Cholangiocarcinoma. Journal of Proteome Research. 2008;7(11):4670-7. doi: 10.1021/pr800215n.
51. Lange S, Sylvester M, Schumann M, Freund C, Krause E. Identification of phosphorylation-dependent interaction partners of the adapter protein ADAP using quantitative mass spectrometry: SILAC vs (18)O-labeling. J Proteome Res. 2010;9(8):4113-22. Epub 2010/06/24. doi: 10.1021/pr1003054. PubMed PMID: 20568816.

Supplemental information captions

Supplementary Information for:

The postsynaptic MAGUK scaffold protein MPP2 organises a distinct interactome that incorporates $GABA_A$ receptors at the periphery of excitatory synapses

Bettina Schmerl[1], Niclas Gimber[2], Benno Kuropka[3], Jakob Rentsch[3], Stella-Amrei Kunde[1], Helge Ewers[3], Christian Freund[3], Jan Schmoranzer[2], Nils Rademacher*[1,4] and Sarah A. Shoichet*[1]

[1] Neuroscience Research Center, Charité – Universitätsmedizin Berlin, Germany, [2] Advanced Medical BioImaging Core Facility – AMBIO, Charité – Universitätsmedizin Berlin, Germany, [3] Institute of Chemistry and Biochemistry, Freie Universität Berlin, Germany, [4] German Center for Neurodegenerative Diseases (DZNE), Berlin, Germany

Correspondence: sarah.shoichet@charite.de

List of supplementary items:

S1 Fig: Dual colour dSTORM images of SynCAM1 and PSD-95.

S2 Fig: Dual colour dSTORM images of MPP2 and PSD-95.

S3 Fig: Dual colour dSTORM images of SynCAM1 and MPP2.

S4 Fig: Nearest neighbour analysis of SynCAM1 and MPP2 protein cluster distances derived from SIM images.

S5 Fig: Validation of novel interaction partners by Co-IP.

S6 Fig: Full-length blots for Fig 4.

S7 Fig: Full-length blots for S5 Fig.

S1 Data: Underlying source data for Fig 3c

S1 Fig: Dual colour dSTORM images of SynCAM1 and PSD-95.

E18 rat primary hippocampal neurons were fixed at DIV21 and stained for endogenous SynCAM1 (magenta) and PSD-95 (cyan) proteins with Alexa Fluor 647 and Cy3b-coupled secondary antibodies. Protein localizations were filtered according to Thompson accuracy, i.e. all localisations with accuracy below 20 nm were excluded. Box size = 750 nm.

S2 Fig: Dual colour dSTORM images of MPP2 and PSD-95.

E18 rat primary hippocampal neurons were fixed at DIV21 and stained for endogenous MPP2 (magenta) and PSD-95 (cyan) proteins with Alexa Fluor 647 and Cy3b-coupled secondary antibodies. Protein localizations were filtered according to Thompson accuracy, i.e. all localisations with accuracy below 20 nm were excluded. Box size = 750 nm.

S3 Fig: Dual colour dSTORM images of SynCAM1 and MPP2.

E18 rat primary hippocampal neurons were fixed at DIV21 and stained for endogenous SynCAM1 (magenta) and MPP2 (cyan) proteins with Alexa Fluor 647 and Cy3b-coupled secondary antibodies. Protein localizations were filtered according to Thompson accuracy, i.e. all localisations with accuracy below 20 nm were excluded. Box size = 750 nm.

S4 Fig: Nearest Neighbour Analysis of SynCAM1 and MPP2 protein cluster distances derived from SIM images. *NN distances from SynCAM1 to the nearest MPP2 cluster were calculated from the cluster centres (upper panel, grey bars) and cluster surfaces (lower panel). Dashed lines represent the upper and lower envelopes of complete spatial randomness (CSR). CSR was calculated by randomly distributing MPP2 within the volume and SynCAM1 on the surface of spheres of 0.8 µm diameter as indicated by the grey dotted line (mean ± SEM, 95% confidence interval, 10 simulations per synapse, N = 3 independent experiments, ~40.000 synapses from 50 images).*

S5 Fig: Validation of novel interaction partners by Co-IP

a) HA-tagged Gnao1 was overexpressed together with EGFP-tagged MPP2 in HEK293T cells. Upon pull-down with Ms αGFP antibody or normal Ms IgG, Gano1 co-purification and GFP pull-down control were detected by Western blot with αHA and αGFP antibodies.

b) Co-IP of FLAG-tagged Arhgef2 together with EGFP-MPP2 after pull-down with αGFP antibody or IgG control, as detected by Western blot using αFLAG and αGFP antibodies.

c) FLAG-tagged Farp1 was overexpressed together with EGFP-tagged MPP2 and co-purifies with αGFP pull-down, as opposed to normal IgG as negative control. Co-IP was detected by Western blot probing with αFLAG and αGFP antibodies.

d) Co-purification of FLAG-tagged Ppp3ca (Calcineurin subunit) overexpressed together with EGFP-MPP2 after αGFP pull-down or normal Ms IgG as negative control, detected by Western blot with αFLAG and αGFP antibodies.

e) EGFP-tagged Pip5k1c was co-expressed with FLAG-tagged MPP2 in HEK293T cells. EGFP-Pip5k1c was precipitated with αGFP antibody or normal IgG as negative control and analysed by Western blot with αFLAG and αGFP antibodies. An additional IgG control lane is marked with an asterisk.

S6 Fig: Full-length blots for Fig 4.

S7 Fig: Full-length blots for S5 Fig.

S1 Data: Underlying source data for Fig 3c.

a

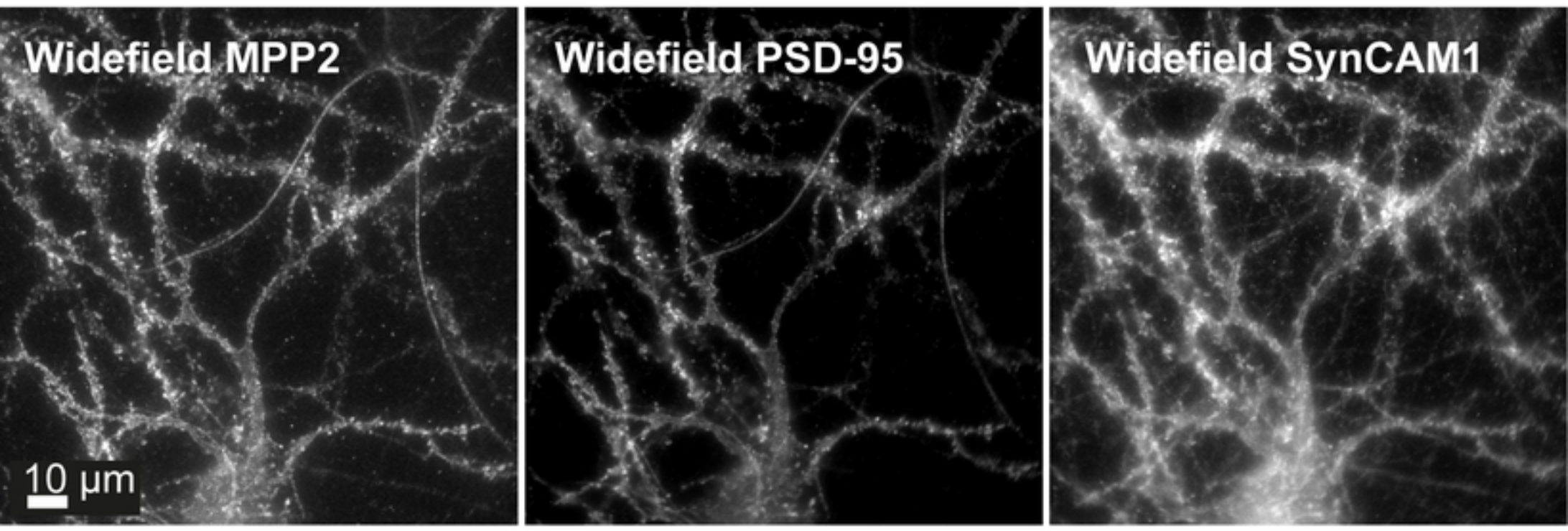

b

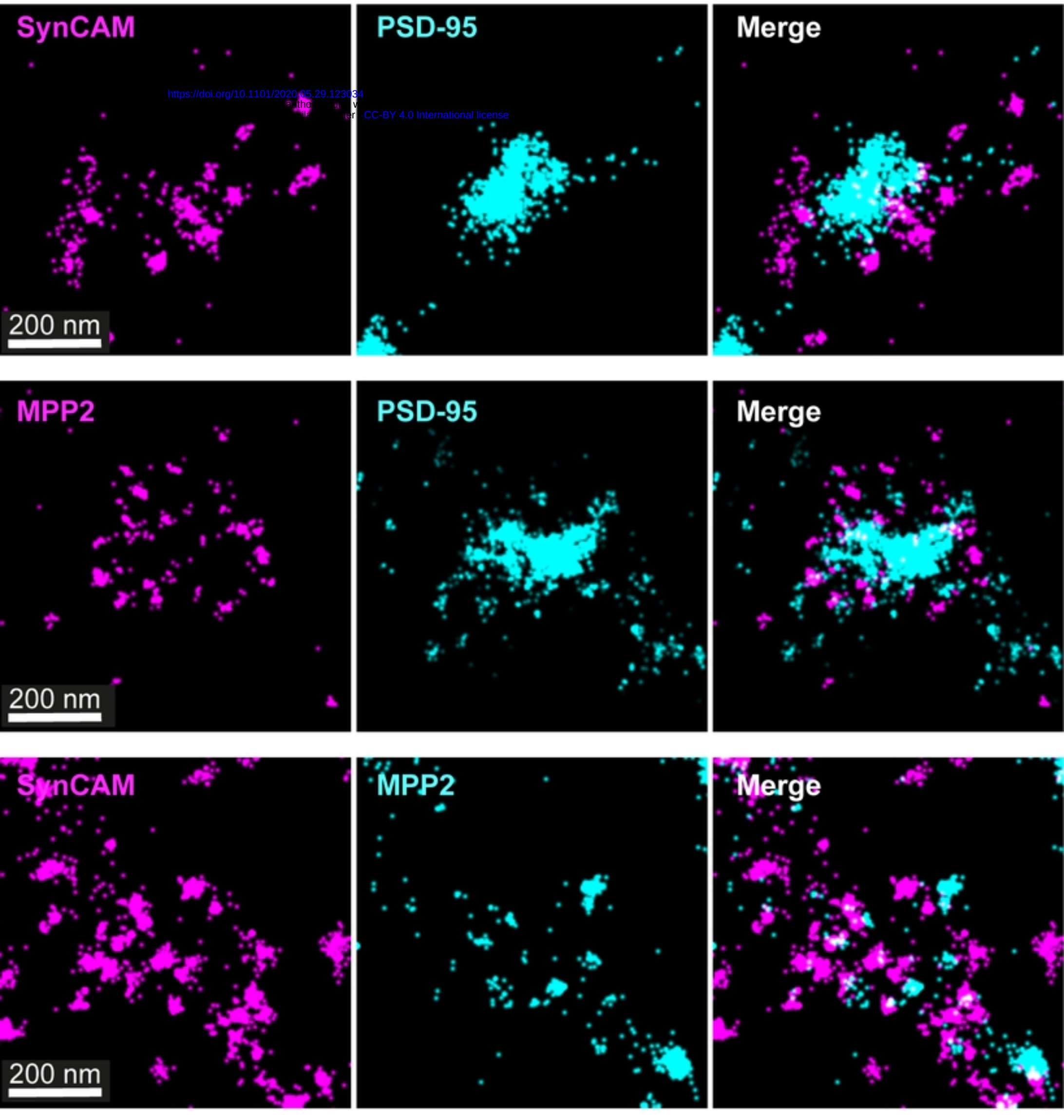

Figure 1

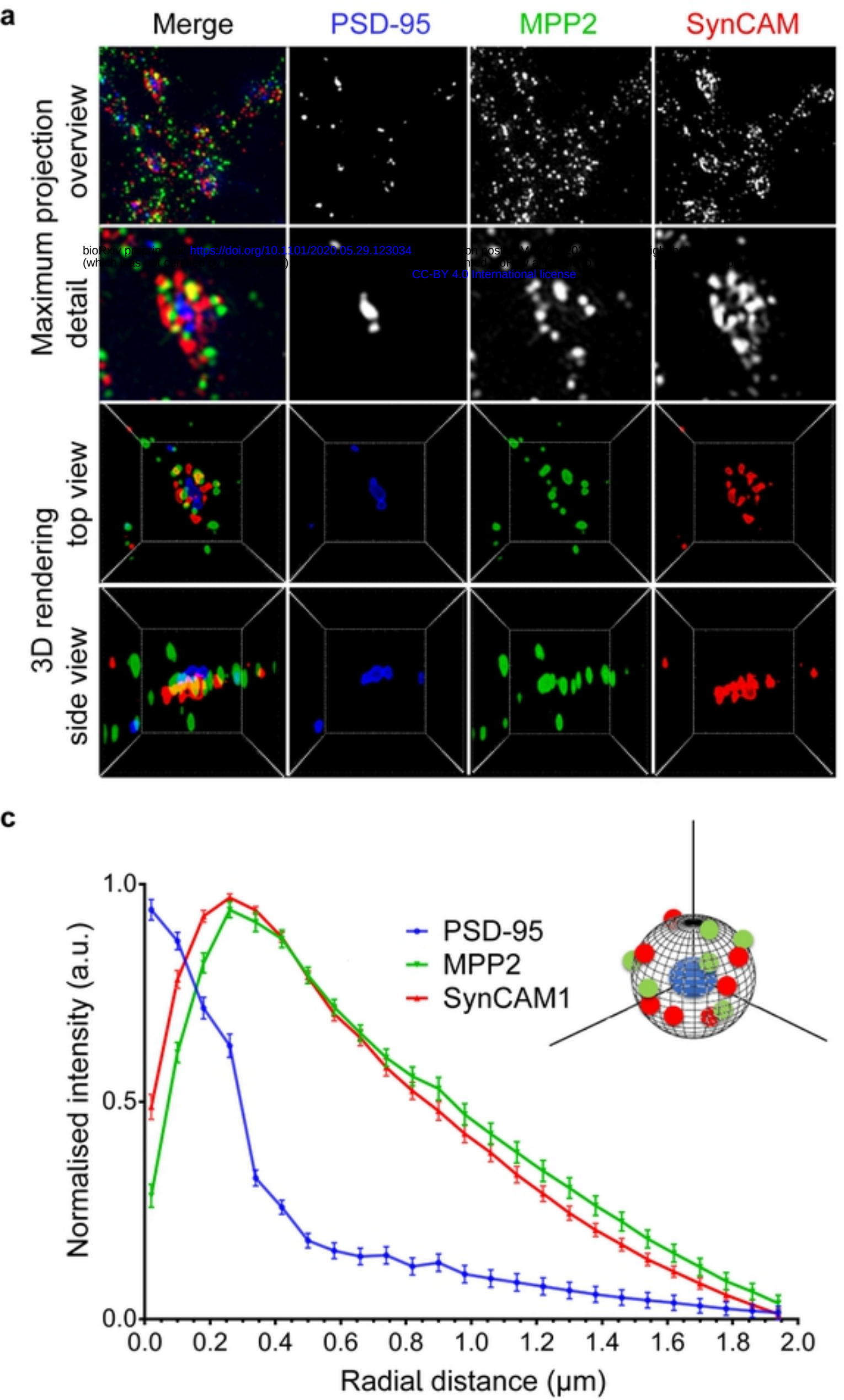

Figure 2

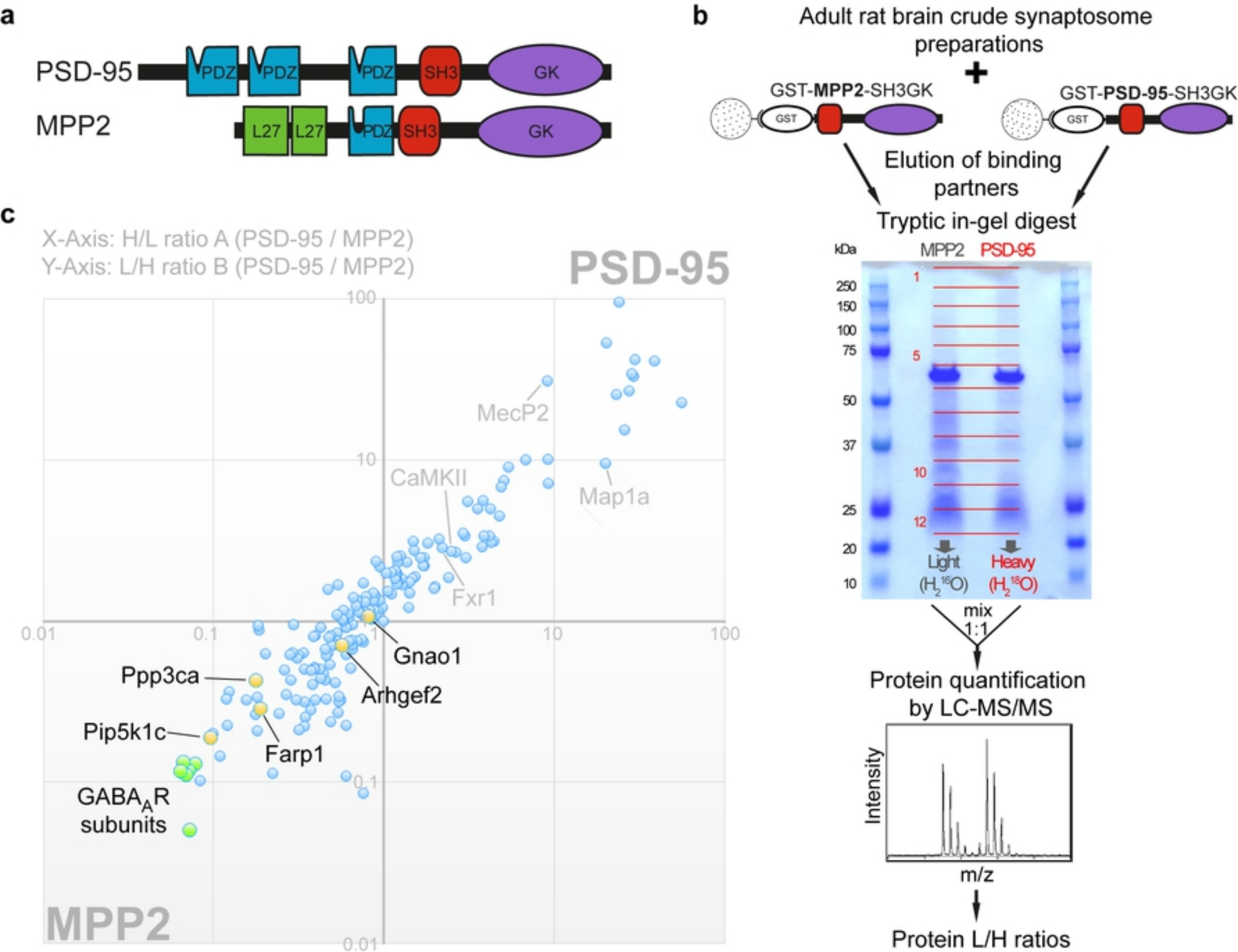
a
PSD-95
PDZ
PDZ
PDZ
SH3
GK
MPP2
L27
L27
PDZ
SH3
GK
b
Adult rat brain crude synaptosome preparations
+
GST-MPP2-SH3GK
GST
GST-PSD-95-SH3GK
GST
Elution of binding partners
Tryptic in-gel digest
kDa
MPP2
PSD-95
250
150
100
75
50
37
25
20
10
1
5
10
12
Light
(H2 16O)
Heavy
(H2 18O)
mix
1:1
Protein quantification
by LC-MS/MS
Intensity
m/z
Protein L/H ratios
c
X-Axis: H/L ratio A (PSD-95 / MPP2)
Y-Axis: L/H ratio B (PSD-95 / MPP2)
PSD-95
MPP2
100
10
1
0.1
0.01
0.01
0.1
1
10
100
MecP2
CaMKII
Map1a
Fxr1
Gnao1
Arhgef2
Ppp3ca
Pip5k1c
Farp1
GABAAR
subunits

Figure 3

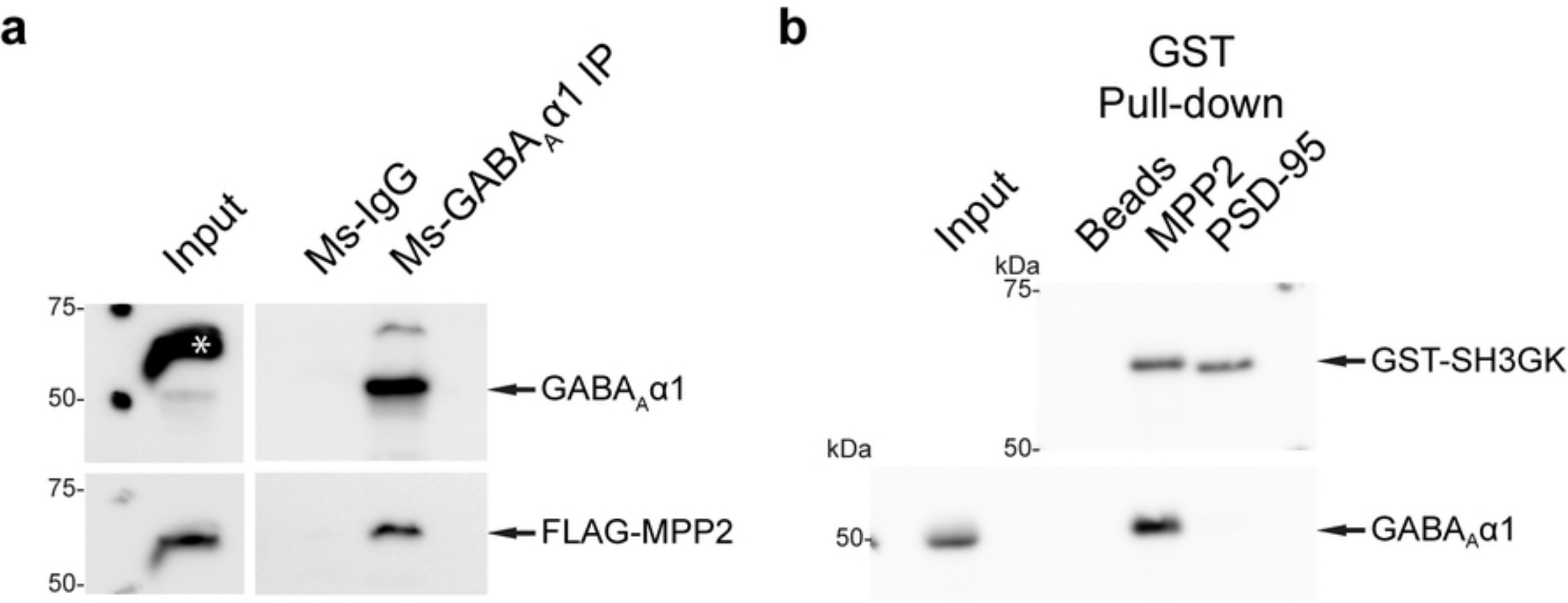
a
Input
Ms-IgG
Ms-GABA$_A$α1 IP
75-
50-
*
GABA$_A$α1
75-
50-
FLAG-MPP2
b
GST
Pull-down
Input
Beads
MPP2
PSD-95
kDa
75-
50-
GST-SH3GK
kDa
50-
GABA$_A$α1

Figure 4

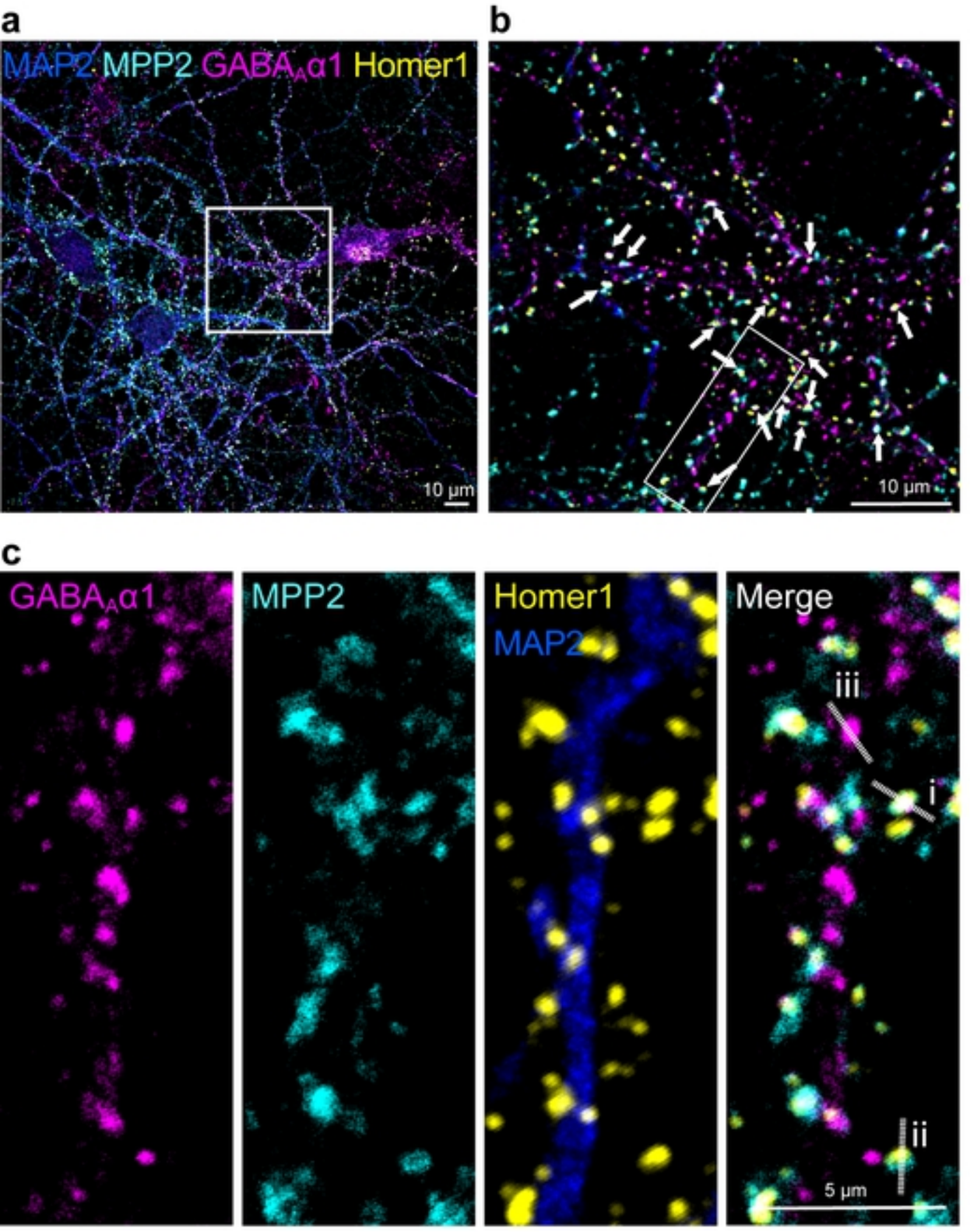
a
MAP2 MPP2 GABA$_A$α1 Homer1
10 µm
b
10 µm
c
GABA$_A$α1
MPP2
Homer1
MAP2
Merge
iii
i
ii
5 µm
d
i) Homer1 / MPP2 / GABA$_A$α1 positive
GABA$_A$α1
MPP2
Homer1
Normalised intensity (a.u.)
Length (µm)
ii) Homer1 / MPP2 positive
Normalised intensity (a.u.)
Length (µm)
iii) GABA$_A$α1 positive
Normalised intensity (a.u.)
Length (µm)

Figure 5

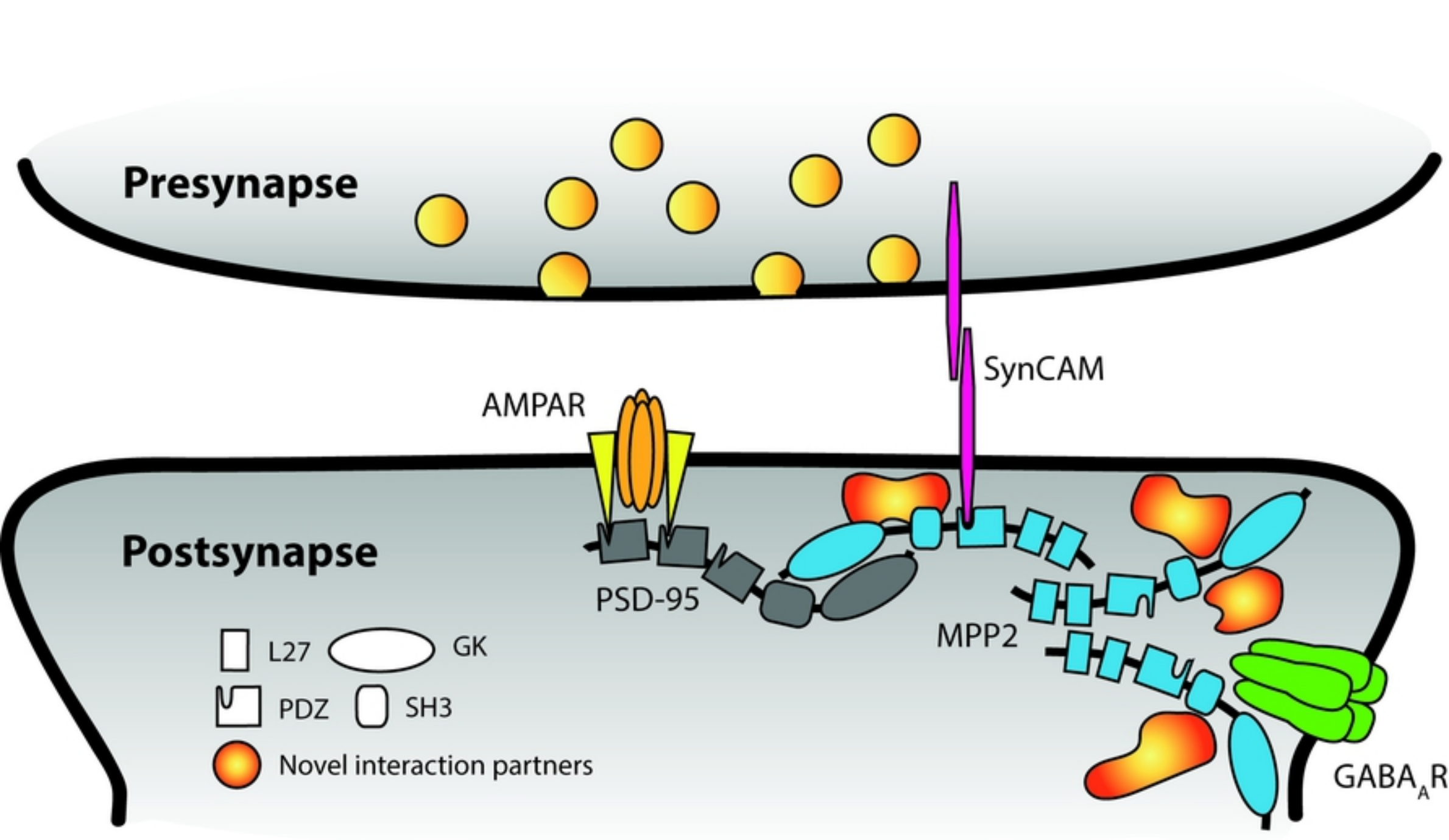
Presynapse
SynCAM
AMPAR
Postsynapse
PSD-95
MPP2
L27
GK
PDZ
SH3
Novel interaction partners
GABA$_A$R

Figure 6